Low-Barrier Hydrogen Bond Hypothesis in the Catalytic Triad Residue of Serine Proteases: Correlation between Structural Rearrangement and Chemical Shifts in the Acylation Process†

Toyokazu Ishida‡

Research Institute for Computational Science, National Institute of Advanced Industrial Science and Technology, Tsukuba Central 2, 1-1-1 Umezono, Tsukuba, 305-8568, Japan, and Department of Chemistry, Graduate School of Science, Kyoto University, Kitashirakawa, Sakyo-ku, Kyoto 606-8502, Japan

Received July 29, 2005; Revised Manuscript Received December 5, 2005

ABSTRACT: To elucidate the catalytic advantage of the low-barrier hydrogen bond (LBHB), we analyze the hydrogen bonding network of the catalytic triad (His57-Asp102-Ser195) of serine protease trypsin, one of the best examples of the LBHB reaction mechanism. Especially, we focus on the correlation between the change of the chemical shifts and the structural rearrangement of the active site in the acylation process. To clarify LBHB, we evaluate the two complementary properties. First, we calculate the NMR chemical shifts of the imidazole ring of His57 by the gauge-including atomic orbital (GIAO) approach within the ab initio QM/MM framework. Second, the free energy profile of the proton transfer from His57 to Asp102 in the tetrahedral intermediate is obtained by ab initio QM/MM calculations combined with molecular dynamics free energy perturbation (MD-FEP) simulations. The present analyses reveal that the calculated shifts reasonably reproduce the observed values for ^{1}H chemical shift of $H_{\epsilon 1}$ and $H_{\delta 1}$ in His57. The ^{15}N and ^{13}C chemical shifts are also consistent with the experiments. It is also shown that the proton between His57 and Asp102 is localized at the His57 side. This largely downfield chemical shift is originated from the strong electrostatic interaction, not a covalent-like bonding character between His57 and Asp102. Also, it is proved that a slight downfield character of $H_{\epsilon 1}$ is originated from a electrostatic interaction between His57 and the backbone carbonyl group of Val213 and Ser214. These downfield chemical shifts are observed only when the tetrahedral intermediate is formed in the acylation process.

Hydrogen bondings play a crucial role in many biological processes (*1*). A special class of them, called the low-barrier hydrogen bond (LBHB[1]), has attracted wide acceptance as a major candidate for efficient enzyme catalysis (*2*−*7*). As two electronegative atoms approach each other within the sum of van der Waals radii, the hydrogen bond becomes stronger and the barrier between the two proton wells becomes lower. When the barrier height approaches the zero-point energy of the hydrogen, the proton becomes delocalized between the two wells; such a state is referred to as the LBHB (*5*, *6*). It has been proposed that LBHB is important in many enzymatic reactions. A typical example is the hydrogen bonding network of the catalytic triad (His57-Asp102-Ser195) of serine proteases (*3*, *4*).

The reaction mechanism of serine proteases has long been a contentious matter (*8*−*10*). Because the hydroxyl group of Ser195 has poor nucleophilicity, how the catalytic triad renders high reactivity to Ser195 has been a matter of controversy. The initially proposed *charge-relay* mechanism (*11*) has been examined by many subsequent studies (^{1}H and ^{15}N NMR (*12*−*15*), neutron diffraction experiments (*16*, *17*), etc.). The unusually low-field proton signal, which was assigned to the proton between His57 and Asp102, was observed in the early NMR experiments (*12*). At present, those signals are considered to be characteristic evidence of the LBHB (*3*, *4*). Frey and co-workers observed an unusually low-field ^{1}H NMR spectrum of ∼19 ppm for the tetrahedral complex of chymotrypsin inhibited by the peptidyl trifluoromethyl ketones (peptidyl-TFKs), which resembles the putative tetrahedral intermediate (*18*). On the basis of the series of experiments, they proposed that the formation of the LBHB between His57 and Asp102 along the catalytic pathway could increase the reactivity of His57 as a general base (*18*−*22*). ^{15}N NMR experiment, however, gave conflicting results about the hydrogen bonding between His57 and Asp102 for the α-lytic protease (*23*).

Ab initio quantum chemical calculations have been applied to study the catalytic triad system of the serine protease family. Westler et al. used the density functional calculations to the model structures of the active site of chymotrypsin (*24*). Though their calculated NMR properties showed reasonable agreement with the experimental data, their models completely neglected the environmental effect of the surrounding protein. To incorporate a structural effect of

† This work was supported by the Grant-in-Aid for Scientific Research, and by the NAREGI Nanoscience Project from the Ministry of Education, Culture, Sports, Science and Technology in Japan.

‡ Phone: +81-29-861-3169. Fax: +81-29-851-5426. E-mail: toyokazu.ishida@aist.go.jp.

[1] Abbreviations: LBHB, low-barrier hydrogen bond; QM/MM, quantum mechanical/molecular mechanical; GIAO, gauge-including atomic orbital; MD-FEP, molecular dynamics free energy perturbation; TSA, transition state analogue; TET, tetrahedral complex; TI, tetrahedral intermediate.

10.1021/bi051515b CCC: $33.50
Published on Web 04/06/2006

protein, Molina and co-workers employed the effective fragment potential (EFP) approach (*25*) to the X-ray structures of α-chymotrypsin and α-lytic protease inhibited by the transition state analogue (*26*, *27*) (TSA). Although their models considered the steric effect of protein, the chemical shift was evaluated by the ONIOM-NMR approach (*28*) that discarded the electrostatic effect from the polar protein environment, which seems to be crucial for the abnormal character of the chemical shift.

There are many physicochemical parameters to be characterized as LBHB (*5*, *6*): a downfield ^{1}H chemical shift, a large primary isotope shift, a low fractionation factor, a close contact in X-ray structures. Among them, the most unambiguous character is considered to be the NMR chemical shift for the proton engaged in the LBHB (*3*, *4*). Though many observations support the formation of LBHB (*18*−*22*), there is no direct connection between the characteristic features of LBHB and its catalytic advantage. The abnormal chemical shift profile of the hydrogen bonding proton needs to be rationalized in some reasonable way if the LBHB hypothesis is not to be invoked. Considering today's experimental/theoretical interpretation which does not reach the generally accepted consensus, calculating the NMR properties of LBHB and the related free energy profile of the proton transfer by a realistic enzyme system must be inevitable to validate the contentious LBHB mechanism.

In this article, we examine the LBHB hypothesis for the catalytic reaction of serine protease trypsin. In order to obtain clear insights, we evaluate two complementary parameters in consistent theoretical calculations: NMR chemical shifts of the imidazole ring of His57 in the catalytic triad and the free energy profile of the proton transfer from His57 to Asp102. Because chemical shifts are determined by electronic currents in a molecule and are sensitive to the protein environment, incorporating the surrounding protein effect is critical to identify the experimentally observed shift. In order to incorporate the steric and electrostatic effect of protein environment on the NMR chemical shifts, we employ the QM/MM technique (*29*−*33*). Most earlier theoretical works considered only one property (chemical shift or related proton-transfer profile) and selected the target system for α-chymotrypsin/α-lytic protease inhibited by TSA, which is the experimental material for LBHB study (*24*, *26*, *27*, *34*−*38*). In contrast to those approaches, here we analyze the acylation process of trypsin to focus on the change of chemical shifts of His57 associated with the change of hydrogen bonding network along the reaction path. Because sterical rearrangement during the catalysis is considered to be a key factor (*18*, *19*, *21*, *23*), a detailed analysis of the chemical shifts during the real reaction process is crucial. Also we discuss the relationship between the chemical shift and the free energy profile, which are evaluated by ab initio QM/MM calculations in a consistent fashion. In contrast to most earlier results which were based on the potential energy profile (*24*, *26*, *27*, *37*), we calculate the free energy profile of proton transfer between His57 and Asp102 with the realistic enzyme system. To clarify the role of His57-Asp102 hydrogen bonding in the catalytic process, we also carry out calculations for the Asn102 mutant reaction as well as the wild-type reaction; the details of its mechanisms are described in the previous two papers (*39*, *40*). Comparing the calculated results with available experimental data, we discuss the assumption of LBHB based reaction mechanism.

1. MATERIALS AND METHODS

1.1. Shielding Tensor Calculations by QM/MM-GIAO. The quantum chemical calculations of NMR chemical shifts and related properties have been discussed in many works (*41*−*44*). Several groups considered the environmental effect on the shielding constants (*45*−*48*). Because the details of methods to calculate the chemical shifts within the framework of QM/MM methodology are described elsewhere (*47*), we give a brief introduction pertinent to the present study.

The chemical shielding tensor is defined as the second-order response to the magnetic field and the nuclear magnetic moment:

$$\sigma^{\mathrm{k}} = \frac{\partial^2 E(\mathbf{B},\mathbf{m}_k)}{\partial \mathbf{B}\, \partial \mathbf{m}_k}\Big|_{\mathbf{B}=0,\mathbf{m}_k=0} = \sum_{\mu\nu} P_{\mu\nu} \frac{\partial^2 H_{\mu\nu}}{\partial \mathbf{B}\, \partial \mathbf{m}_k} + \sum_{\mu\nu} \frac{\partial P_{\mu\nu}}{\partial \mathbf{B}} \frac{\partial H_{\mu\nu}}{\partial \mathbf{m}_k} \quad (1)$$

where $\mathbf{B}$ is the external magnetic field and $\mathbf{m}_k$ is the nuclear magnetic moment of atom k, respectively. We employed the gauge-including atomic orbital (GIAO) approach (*49*, *50*) to calculate eq 1. In the GIAO, the shielding tensor is calculated with the use of the field dependent basis functions.

In the present study, we employed the Hartree−Fock (HF) wave function to describe the QM region. The QM/MM interaction Hamiltonian is of the form

$$\hat{H}_{\mathrm{QM/MM}} = \hat{H}^{\mathrm{elec}}_{\mathrm{QM/MM}} + \hat{H}^{\mathrm{vdw}}_{\mathrm{QM/MM}} + \hat{H}^{\mathrm{strain}}_{\mathrm{QM/MM}} \quad (2)$$

where the first term is treated by the one-electron operator in the QM region calculations, while the second and third ones represent the van der Waals interaction between the QM/MM regions and the strain energy at the QM/MM boundaries, respectively. The second and third terms are evaluated by the MM force field with the AMBER (parm.96) potential functions (*51*, *52*). Because we only considered the electrostatic effect originated from the partial charges assigned on the MM atomic sites, the perturbation effect from the MM region was introduced through the density matrix and its derivative. The density matrix $P_{\mu\nu}$ was determined from the converged QM/MM wave function, and the derivative of $P_{\mu\nu}$ with respect to the magnetic field $\mathbf{B}$ was solved via the CPHF equation (*53*). With these modifications, the chemical shielding tensor was calculated within the QM/MM framework.

1.2. Free Energy Profile along the Reaction Path. The total free energy profile is calculated along the selected reaction coordinate by the following approximation (*39*, *40*, *54*):

$$F \simeq G_{\mathrm{QM}}(\mathbf{R}^{\mathrm{min}}_{\mathrm{QM}}) - k_{\mathrm{B}}T \ln \int \mathrm{e}^{-\beta[E_{\mathrm{QM/MM}}(\mathbf{R}^{\mathrm{min}}_{\mathrm{QM}},\mathbf{R}_{\mathrm{MM}})+E_{\mathrm{MM}}(\mathbf{R}_{\mathrm{MM}})]}\, \mathrm{d}\mathbf{R}_{\mathrm{MM}} \quad (3)$$

The first term represents the vibrational free energy in the QM region, and the second is the free energy contribution from the MM region (surrounding protein and solvent).

$\mathbf{R}_{QM}^{min}$ means the optimized geometry on the selected reaction coordinate in the QM region. In contrast to the related works (*54*−*56*), the internal degrees of freedom in QM region are exactly fixed at the QM/MM optimized one by using the constrained-MD technique. The QM geometry is projected onto the predefined reaction coordinate and is forced to transform adiabatically from reactant to product structure during the MD run. The perturbed states (both forward and backward directions), whose structures are also exactly retained predefined reaction path optimizations, are generated to calculate the free energy difference in each MD step. To achieve enough configuration sampling, MD simulations are performed in a classical manner, where electrostatic interactions between QM and MM regions are approximated by the RESP charge model (*57*, *58*). RESP charges in the QM region are optimized to reproduce QM/MM reaction path results. In this way, the QM/MM results are incorporated into the simulation. The MM contribution of the free energy term is evaluated by the FEP-like manner (*59*) along the defined reaction path determined before free energy simulation. This real *chemical perturbation* along the reaction path guarantees the good convergence of the free energy difference during the MD run. The QM free energy is estimated by ab initio QM/MM force constant calculations based on the harmonic approximation. The details of the calculations were described in the previous papers (*39*, *40*).

1.3. Definition of the Molecular Systems. The molecular systems (wild-type/Asn102-mutant trypsin-substrate complex) were adopted from the QM/MM optimized geometries along the reaction path, obtained from the earlier results (*39*, *40*). In the case of the wild-type reaction, the acylation reaction progresses in the following way. After the formation of the ES complex, the reaction starts accompanying with the concerted two reactive modes (the proton transfer from Ser195 to His57 and the nucleophilic attack of Ser195 to the scissile peptide of the substrate), and the resultant tetrahedral complex (TET) is formed. For the reaction to proceed further, TET must be converted into the structure (TET′) preferable to abstract the proton from His57. Then TET′ breaks down into the product acylenzyme (EA) accompanied by the two concerted reactive modes (the proton transfer from His57 to the scissile amide and the cleavage of the scissile peptide bond). We identified TET′ as the putative tetrahedral intermediate (TI), while TET as an artificial structure originated from the limitation of the QM/MM optimizations (*39*). It is however noted that the TET structure also resembles the experimental structure of the TI of chymotrypsin inhibited by the peptidyl-TFKs. We therefore calculated the chemical shifts at the TET geometry as well as the TET′ one. Two transition state structures (TS and TS′) are observed during the formation and breakdown of the tetrahedral intermediate, respectively.

We focused here on the chemical shifts of the hydrogen bonding network of the catalytic triad residue at the characteristic point (ES, TI, EA, etc.) along the reaction path. The QM region adopted here contains the side chains of the catalytic triad (His57, Asp102, and Ser195), the backbone carbonyl group of Val213, the whole of Ser214, and the backbone NH group of Trp215, as well as the scissile peptide of the substrate (peptide bond between substrate Arg5 and Ile6) as seen in Figure 1. Note that Asp102 was replaced by Asn102 for the mutant reaction. The boundaries between the QM and MM regions ($C_\alpha-C_\beta$ bond of His57 and Asp102 (or Asn102), C_α−NH, C_α−CO bonds of Ser195, $C_\alpha-C_\beta$, C_α−NH bonds of substrate Arg5, $C_\alpha-C_\beta$, C_α−CO bonds of substrate Ile6, C_α−CO bond of Val213, and C_α−NH bond of Trp215) were saturated by link hydrogen atoms. In all chemical shift calculations, we employed the 6-31(+)G*(*) basis set (*60*) (diffuse functions were added to the carboxylic group of Asp102, O_γ of Ser195 and Ser214, the scissile peptide portion of the substrate, and p-functions were added to H_γ of Ser195 and Ser214, $H_{\delta 1}$ of His57). No cutoff was introduced between QM and MM interactions.

FIGURE 1: The definition of the QM region used in the chemical shift calculations. The residues colored by green are the side chains of the catalytic triad (His57, Asp102, and Ser195); purple designates the backbone carbonyl group of Val213, the whole of Ser214, and the NH group of Trp215; yellow designates the scissile peptide portion of the substrate (peptide bond between Arg5 and Ile6). The structure is adopted from the QM/MM optimized structure of the wild-type ES complex used in the previous work (*39*).

For the reference compounds of chemical shift, we chose tetramethylsilane (TMS) for ^1H and ^{13}C chemical shifts and NH_3 for ^{15}N. The relative shifts were evaluated by using the chemical shifts of the reference compounds optimized at HF/6-31G**. The observed chemical shifts are given by the ensemble average of many configurational states in a given temperature. In the case of the strong hydrogen bonds whose observed shifts largely depend on the nuclear position on the related potential surface, a consideration of the configurational averaging might be an important factor. At present, however, the calculation of the dynamical averaging shifts based on ab initio methods is too demanding for the present molecular system. Therefore, we estimated the thermal averaged proton chemical shift based on the free energy profile combined with the corresponding shielding surface.

The calculation details of the free energy profile are as follows. The minimum energy path was first determined by ab initio QM/MM calculations. Starting the QM/MM optimized geometry of the tetrahedral intermediate (TET′) structure, the reaction path was calculated by the geometry optimizations. We chose 13 different values for the His57 $N_{\delta 1}-H_{\delta 1}$ bond distance, and the optimizations were carried

Table 1: The Calculated Chemical Shifts δ (ppm) at the Characteristic Point along the Acylation Path for the Wild-Type Reaction[a]

	ES	TS	TET[b]	TI (=TET′)	TS′	EA
$\delta_{H\delta1}$ of His57	15.5	17.6	18.9	17.8	14.7	13.5
$\delta_{H\delta2}$ of His57	5.6	5.6	5.8	6.0	6.1	5.8
$\delta_{H\epsilon1}$ of His57	7.9	8.5	8.8	8.7	8.8	7.7
$\delta_{N\delta1}$ of His57	167.9	171.6	176.0	172.5	167.1	162.9
$\delta_{N\epsilon2}$ of His57	226.5	176.3	159.0	161.1	169.1	244.5
$\delta_{C\gamma}$ of His57	125.8	127.8	129.3	128.8	130.1	126.0
$\delta_{C\delta2}$ of His57	118.7	110.3	109.6	110.0	111.3	120.9
$\delta_{C\epsilon1}$ of His57	141.7	142.6	142.7	142.0	141.6	138.6

[a] All chemical shifts were calculated by ab initio QM/MM-GIAO HF/6-31(+)G*(*) level, based on the optimized structures along the acylation reaction path. The definition of the reaction coordinate and the discussion of the reaction mechanism were described in the previous work (*39*). [b] TET was an artificial structure originated from the limited availability of QM/MM optimizations.

Table 2: The Calculated Chemical Shifts δ (ppm) at the Characteristic Point of the Asn102 Mutant Reaction[a]

	ES	TET
$\delta_{H\delta1}$ of His57	10.8	12.0
$\delta_{H\delta2}$ of His57	5.9	6.1
$\delta_{H\epsilon1}$ of His57	7.6	8.8
$\delta_{N\delta1}$ of His57	157.2	161.7
$\delta_{N\epsilon2}$ of His57	243.4	170.1
$\delta_{C\gamma}$ of His57	122.7	126.4
$\delta_{C\delta2}$ of His57	121.5	113.4
$\delta_{C\epsilon1}$ of His57	138.8	141.2

[a] All chemical shifts were calculated by ab initio QM/MM-GIAO HF/6-31(+)G*(*) level, based on the optimized structures along the acylation reaction path. The definition of the reaction coordinate and the discussion of the reaction mechanism were described in the previous work (*40*).

out for all the remaining degrees of freedom with fixing the $N_{\delta1}-H_{\delta1}$ bond distance. Note that all geometry optimizations were performed in the internal coordinate space, where the donor and acceptor bond lengths of the proton transfer, as well as the structural rearrangement of the acylation reaction, were explicitly considered. In these calculations, the QM region was limited to the side chains of the catalytic triad and the scissile peptide portion of the substrate as used in the previous papers (*39*, *40*). In all MD-FEP calculations, the same solvated system was adopted used in the previous works. A total of 12 windows were used. In each window, the simulation consisted of a 10 ps equilibration process followed by a 30−50 ps averaging run. The relative free energies were calculated as the average of the forward/backward simulation results.

2. RESULTS AND DISCUSSION

2.1. Chemical Shifts along the Acylation Process. The calculated chemical shifts at the critical points along the reaction path in the wild-type reaction are summarized in Table 1. Those of the TET formation step for the Asn102 mutant reaction are also given in Table 2.

As seen in Table 1, the chemical shift of $H_{\delta1}$ is largely downfield compared with those of the other protons of His57 ($H_{\delta2}$ and $H_{\epsilon1}$) at the ES complex of the wild-type reaction. A downfield character of $H_{\delta1}$ shift is also observed for the ES complex of the mutant reaction, though the degree of deshielding is smaller than that of the wild type (Table 2). These results indicate that the chemical environment around $H_{\delta1}$ is different from those of the other protons. In order to see the effect of the Asp102 or Asn102 residue on the proton chemical shifts, we carried out calculations for the model dimer complex of imidazole and ethanol, which mimics the hydrogen bonding system of His57 and Ser195 without the Asp102/Asn102 residue. The resultant chemical shift was 8.4 ppm for the imidazole $H_{\delta1}$. Considering that the hydrogen bond distance is comparable between the wild-type (2.723 Å) and Asn102 mutant (2.834 Å) reactions, the large downfield character of $\delta_{H\delta1}$ for the wild type is mainly attributed to the electrostatic effect on the hydrogen bonded $H_{\delta1}$ originating from the negative charge on the carboxyl group of Asp102. Because a proton engaged in a strong hydrogen bonding is considered to be deshielded by at least 5 ppm (*6*), the His57 and Asp102 residues are regarded to form a moderately strong hydrogen bond even in the ES complex.

The $H_{\delta1}$ chemical shift in Table 1 increases along the reaction path and reaches its maximum value at the tetrahedral intermediate, followed by the decrease from the intermediate to the EA complex. A slight upfield shift at the TET′ complex from TET (from 18.9 to 17.8 ppm) is due to the change of hydrogen bond distance between His57 and Asp102 by the conversion from the TET structure (2.605 Å) to TET′ (2.650 Å). In the EA state, the strong hydrogen bonding observed at the tetrahedral intermediate disappears and the chemical shift becomes 13.5 ppm. The other proton chemical shifts also slightly change along the reaction path. The $H_{\epsilon1}$ shift moves to the downfield direction when the tetrahedral intermediate is formed. This is consistent with the structural change that the protonated His57 forms a kind of hydrogen bonding with the backbone carbonyl groups of Val213 and Ser214. Compared with the wild-type reaction, the magnitude of downfield in the $H_{\delta1}$ shift from the ES to TET is smaller for the Asn102 mutant reaction, indicating that the hydrogen bonding at TET for the mutant reaction is not so strong as the wild-type reaction. This result is consistent with the reaction free energy profile of the Asn102 mutant reaction, whose main anticatalytic factor is the loss of the strong electrostatic interaction between His57 and Asn102 (*40*). However, the downfield character of the $H_{\epsilon1}$ shift is quite similar to that of the wild-type reaction. The previous work clearly revealed that, to compensate a large loss of the electrostatic stabilization between His57 and Asn102, the mutant enzyme uses an attractive interaction with Ser214 to decrease the total reaction free energy. The present results also show the importance of remote site interaction for the efficient catalysis.

Experimentally, the related proton chemical shifts were measured based on the tetrahedral analogues of chymotrypsin, inhibited by the peptidyl-TFKs (*18*−*22*). Though the chemical shift varies with the structure of the peptidyl groups, $\delta_{H\delta1}$ of the tetrahedral analogues is 18.6−19.0 ppm, while that of the neutral His57 (corresponding to the ES complex) is ∼15 ppm. Also the observed shift of $\delta_{H\epsilon1}$ is within the range of 9.0−9.2 ppm. The calculated proton chemical shifts for the tetrahedral intermediate (TET/TET′) are in good agreement with these experimental values for both the $H_{\delta1}$ and $H_{\epsilon1}$ protons.

We tabulated the calculated ^{15}N and ^{13}C chemical shifts along the reaction path both for the wild-type and Asn102 mutant reactions in Table 1 and 2. For the wild-type reaction, the chemical shift of $N_{\epsilon 2}$ in His57 shows a large decrease at the tetrahedral intermediate (67.5 and 65.4 ppm for TET and TET′, respectively) compared with the ES complex, while that of $N_{\delta 1}$ increases slightly. The same trend was also observed for the mutant reaction. These results are consistent with the experiments by Bachovchin and co-workers for α-lytic protease (*23*, *62*, *63*). The experimental $N_{\delta 1}$ and $N_{\epsilon 2}$ chemical shifts are 185.9 and 173.5 ppm for the protonated state corresponding to the tetrahedral intermediate, while those for the neutral one corresponding to the ES complex are 178.1 and 239.5 ppm, respectively. As for the ^{13}C chemical shifts of α-lytic protease, Sudmeier et al. reported that $\delta_{C\delta 2}$ of His57 undergoes a large downfield shift of 6.2 ppm during the change of pH from 4.0 to 9.0 (*64*). In accordance with the experiment, the calculated $\delta_{C\delta 2}$ decreases from 118.7 ppm at ES to 109.6 or 110.0 ppm at TET or TET′.

It is noted that we employed the HF approximation to calculate the NMR chemical shifts. The inclusion of electron correlation effect with a larger basis set may be required to compare with the experimental values more quantitatively, particularly for ^{15}N and ^{13}C chemical shifts (*65*). In spite of a limitation of the present calculations, the resultant chemical shifts are consistent with the available experiments.

2.2. Free Energy Profile of Proton Transfer. In the LBHB hypothesis, the hydrogen bonded proton moves on a double well potential and is shared by two electronegative atoms. In order to examine the validity of the LBHB hypothesis in the present trypsin catalytic reaction, we calculated the free energy curve for the proton transfer from His57 to Asp102.

Figure 2 (upper panel) shows the free energy profile along the proton-transfer coordinate, the $N_{\delta 1}-H_{\delta 1}$ distance of His57. The components of reaction free energy are summarized in Table 3. The calculated free energy curve has a single well at the $N_{\delta 1}-H_{\delta 1}$ distance of 1.093 Å with the N−O distance being 2.605 Å, indicating that the hydrogen bonded proton is localized at the His57 side and not shared by the two residues. Although the free energy contribution from the QM part is more stable at the product side where the proton is bonded to Asp102, the electrostatic interaction with the protein and solvent environments largely stabilizes the reactant. The importance of electrostatic stabilization at the tetrahedral intermediate is also the key factor to prevent the concerted double proton transfer (so-called the *charge-relay*) mechanism during the acylation process, as discussed in the previous work (*40*). Topf et al. employed direct ab initio QM/MM MD simulation of the tetrahedral intermediate of elastase in the deacylation step to calculate the free energy curve for the proton-transfer reaction (*38*). In contrast to the present result, they found a minimum at the product side with the energy higher by ∼1.6 kcal/mol than that of the reactant. Though the present reaction system is different from that of Topf et al., the lack of the product potential well in the present calculations might be attributed to the harmonic approximation in estimating the free energy contribution of the QM region, which cannot take account of large geometric displacements from the optimized minimum energy path. In spite of the difference in the free energy profile, both the

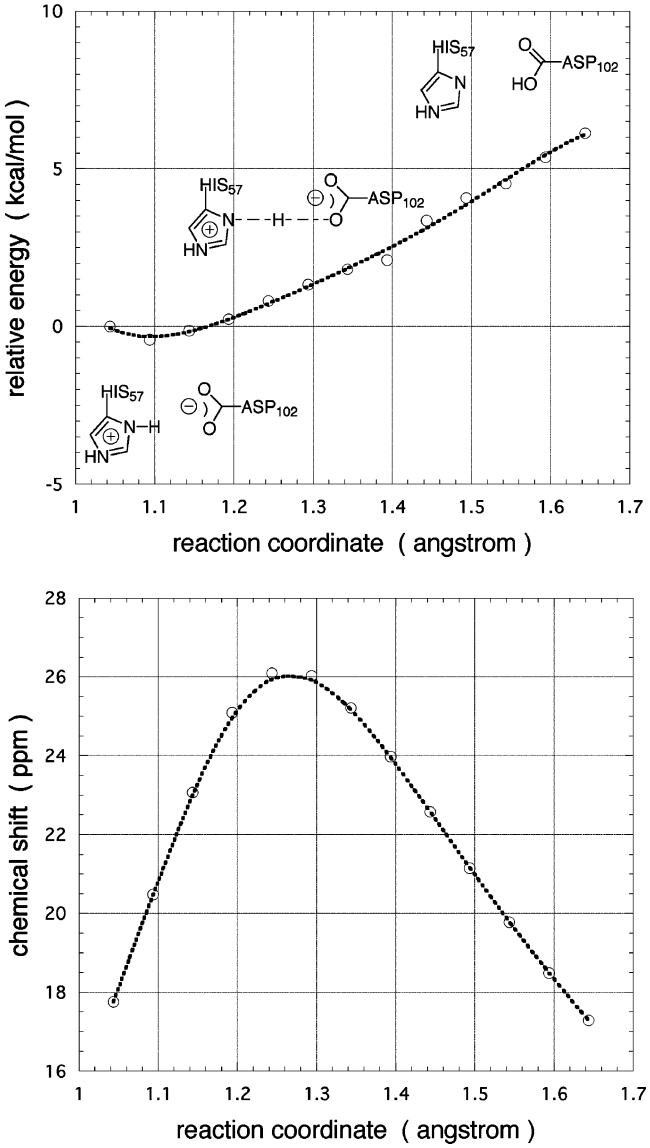

FIGURE 2: The proton transfer from His57 to Asp102 in the tetrahedral intermediate. Upper panel: The free energy profile as the function of the reaction coordinate ($N_{\delta 1}-H_{\delta 1}$ bond distance of His57). Lower panel: The related chemical shift ($\delta_{H\delta 1}$) profile as the function of the reaction coordinate. The reactant was chosen as the QM/MM optimized TET′ structure.

calculations concluded that the proton is localized at the His57 side.

The $H_{\delta 1}$ chemical shift along the proton-transfer path is shown in Figure 2 (lower panel). The shift moves to the downfield direction with the increase of $N_{\delta 1}-H_{\delta 1}$ distance and becomes the maximum at ∼1.25 Å, followed by the upfield shift with approaching the proton to Asp102. The chemical shift at the minimum free energy point is 20.5 ppm. We also calculated the thermally averaged chemical shift by weighting the Boltzmann distribution estimated from the calculated free energy curve, and the result was 21.6 ppm. Note that although QM/MM-GIAO calculations incorporate the environmental effect of the protein, the electrostatic interaction originated from the enzyme is a minor factor for the calculated shift. The change of chemical shift along the reaction coordinate is mainly correlated to N−H bond distance.

2.3. Low-Barrier Hydrogen Bond Hypothesis. The LBHB hypothesis postulates that the hydrogen bonded proton is

Table 3: Free Energy Calculation Results of the Proton Transfer from His57 to Asp102 at the Tetrahedral Intermediate (kcal/mol)

	Asp-COO$^-$ H-His → Asp-COOH His
QM part contribution[a]	−5.06
(E(QM) part)	(−6.32)
(E_{MP2})	(2.36)
(ZPE)	(−0.59)
(TΔS)	(0.51)
protein contribution[b]	8.46 ± 0.32
solvent contribution[b]	2.74 ± 0.09
total free energy[b]	6.14 ± 0.41

[a] In all QM/MM reaction path calculations, the QM region was limited to the side chains of the catalytic triad and the scissile peptide portion of the substrate as used in the previous works (*39*, *40*). The QM/MM geometry optimizations were performed at the HF/6−31(+)G*(*) level. The electron correlation energy at each optimized point was evaluated by the single point MP2 calculation with the (aug)-cc-pVDZ basis set (*61*), augmented by diffuse functions on the related atoms (the carboxylic group of Asp102, O_γ of Ser195, and the scissile peptide portion of the substrate). ZPE and entropy contributions were calculated by the numerical differentiation method at the HF/6-31(+)G*(*) level in 310 K (0.89 scale factor was employed). [b] The error estimates indicate the difference between the forward and backward MD-FEP simulation runs.

equally shared by two electronegative atoms. The origin of unusually downfield character for the proton chemical shift is considered to the attenuation of the electronic shielding around the proton by forming the hydrogen bonds with the two electronegative atoms. This is consistent with the results in Figure 2 (lower panel) that the ^{1}H chemical shift increases along the proton-transfer path and becomes ∼26 ppm at the point where the distances of the proton from the N and O atoms are comparable and the N−O distance is shortened. However, the present calculations show that the free energy profile of the proton between His57 and Asp102 is of a single well and the proton is localized at the His57 side. In spite of the single well free energy profile, the calculated $\delta_{H\delta1}$ at the tetrahedral intermediate showed a large downfield character of 20.5 ppm (at the free energy minimum), which agrees with the experiments. The ^{15}N and ^{13}C chemical shifts are also consistent with the available experimental ones.

To judge the catalytic proposal of LBHB based only on the NMR chemical shifts is not a conclusive way. For example, Garcia-Viloca et al. analyzed the hydrogen bonds in the hydrogen maleate and hydrogen malonate anions, which are experimentally characterized as LBHB (*66*). Their results showed that although LBHB will always have a downfield chemical shift, the opposite statement is not necessarily true. As stated by Warshel and co-workers, who concluded that the delocalized charge of a symmetric LBHB is an anticatalytic factor because it leads to a large reduction of the electrostatic free energy by the polar environment (*34*, *35*), it is of great importance to discuss the free energy profile of the proton transfer, which corresponds to the pK_a difference between donor and acceptor (*36*). The present calculated free energy profile based on the realistic reaction model shows an apparent asymmetric character. Based on the series of ^{1}H NMR experiments, Frey and co-workers suggested the importance of the conformational compression induced by the substrate binding, which brings the formation of LBHB between His57 and Asp102 (*18*−*22*). In the series of our theoretical analysis of the acylation process, however, no apparent large conformational effect is observed during the catalytic process (*39*, *40*). In spite of no large steric compression, the present calculations reproduced the large downfield NMR character. Considering these results, one can conclude that the abnormal chemical shift at the tetrahedral intermediate in the serine protease catalytic reaction is rationalized without assuming the LBHB hypothesis. The unusually downfield profile is mainly originated from the strong electrostatic interaction between the protonated His57 and Asp102.

In the previous two papers (*39*, *40*), we proposed the reaction mechanism based on the electrostatic stabilization of the tetrahedral intermediate formed along the catalytic pathway. The main source of the electrostatic factor is originated from the multiple hydrogen bonds at the active site. The calculated downfield chemical shifts which imply the formation of the hydrogen bondings strengthen the proposed mechanism. The most problematic point of the reaction mechanism of serine proteases is an unlikely reactivity of Ser195 as a nucleophile for the peptide hydrolysis (*9*, *10*). The present results show that $H_{\delta1}$ of His57 in the wild-type reaction is exerted by the strong electrostatic effect of the adjacent Asp102 even in the ES complex. Although the original *charge-relay* proposal (*11*), where the reactivity of Ser195 is rendered through the resonance forms of Asp-COO$^-$ H-His Ser-OH ⇌ Asp-COOH His-H Ser-O$^-$, has not gained wide acceptance, the series of works clearly show that the hydrogen bonding between His57 and Ser195 is strengthened through that between His57 and Asp102. When the tetrahedral intermediate is formed, the negative charge is concentrated on the oxyanion while the resultant positive charge is developed on the imidazole ring of His57. As was clarified in the second paper which compared the catalytic factor between the wild type and the Asn102 mutant (*40*), the positive charge on the protonated His57 is stabilized by two different factors. One is the strong hydrogen bond formed between His57 and Asp102. The calculated properties validate the strong electrostatic effect between His57 and Asp102. The other is a kind of hydrogen bonding formed between His57 on one domain and the backbone carbonyl groups located on another domain during the catalysis. The slightly downfield character of $\delta_{H\epsilon1}$ in His57 is consistent with this structural change. The importance of this type of hydrogen bond is pointed out by Derewenda et al. on the basis of the extensive comparative study of serine hydrolases (*67*). To answer the effective catalysis, Bachovchin and co-workers proposed the His57-ring-flip mechanism (*23*, *68*), whose experimental evidence largely depends on the downfield shift of $\delta_{H\epsilon1}$ in His57. The series of our theoretical works reveal that the electrostatic stabilization among two domains is a critical element for the effective catalysis, and the downfield character of $\delta_{H\epsilon1}$ is originated from this remote site interaction, not the ring-flipping process that accompanies the disruption and re-formation of the hydrogen bonding network. This result agrees with the QM/MM MD simulations of the tetrahedral intermediate of elastase by Topf et al. (*38*).

3. CONCLUSION

In this article, we have calculated the NMR chemical shifts of the catalytic triad residue of serine protease trypsin by ab initio QM/MM-GIAO method, and also estimated the free energy profile of the proton transfer between His57-Asp102

dyad in the tetrahedral intermediate by using QM/MM combined with MD-FEP simulations. We focus here on the correlation between the chemical shifts and the structural rearrangement of the active site in the acylation step. The present results show that an apparent downfield character of $H_{\delta 1}$ shift is observed when the tetrahedral intermediate is formed. The calculated free energy profile of the proton transfer from His57 to Asp102 at the tetrahedral intermediate shows an asymmetric single well character, where the hydrogen bonding proton is localized on the His57 side. In spite of this free energy profile, the proton chemical shift of $\delta_{H\delta 1}$ in His57 shows an unusually downfield value. This result is mainly originated from the strong electrostatic interaction between the protonated His57 and the ionized Asp102, which deshield the electronic environment of the hydrogen bonding proton. Although the abnormal electrostatic environment between His57 and Asp102 largely influences the electronic character of the proton on His57, the downfield shift is more correlated to the N−H bond distance of the imidazole ring of His57. The present analyses clearly reveal that an unusually downfield proton chemical shift is rationalized based on the concept of *electrostatic stabilization*, without invoking the LBHB hypothesis which postulates the symmetric double well potential with the delocalized proton.

Also, the present results show that the chemical shift of $H_{\epsilon 1}$ in His57 shows a slightly downfield character when the tetrahedral intermediate is formed. These results clarify the importance of the electrostatic stabilization of the tetrahedral intermediate formed in the acylation process.

ACKNOWLEDGMENT

The author is grateful to Dr. Akihiro Morita for his valuable comments and continuous encouragement. The numerical calculations were carried out on the Computer Center of the Institute for Molecular Science (IMS).

REFERENCES

1. Jeffrey, G. A., and Saenger, W. (1991) *Hydrogen Bonding in Biological Structures*, Springer-Verlag, Berlin.
2. Cleland, W. W., and Kreevoy, M. M. (1994) Low-Barrier Hydrogen Bonds and Enzymic Catalysis, *Science 264*, 1887−1890.
3. Frey, P. A., Whitt, S. A., and Tobin, J. B. (1994) A Low-Barrier Hydrogen Bond in the Catalytic Triad of Serine Proteases, *Science 264*, 1927−1930.
4. Cleland, W. W., Frey, P. A., and Gerlt, J. A. (1998) The Low Barrier Hydrogen Bond in Enzymatic Catalysis, *J. Biol. Chem. 273*, 25529−25532.
5. Perrin, C. L., and Nielson, J. B. (1997) "Strong" Hydrogen Bonds in Chemistry and Biology, *Annu. Rev. Phys. Chem. 48*, 511−544.
6. Mildvan, A. S., Harris, T. K., and Abeygunawardana, C. (1999) Nuclear Magnetic Resonance Methods for the Detection and Study of Low-Barrier Hydrogen Bonds on Enzymes, *Methods Enzymol. 308*, 219−245.
7. Harris, T. K., and Mildvan, A. S. (1999) High-Precision Measurement of Hydrogen Bond Lengths in Proteins by Nuclear Magnetic Resonance Methods, *Proteins: Struct., Funct., Genet. 35*, 275−282.
8. Fersht, A. (1999) *Structure and Mechanism in Protein Science: A Guide to Enzyme Catalysis and Protein Folding*, 2nd ed., W. H. Freeman and Company, New York.
9. Wharton, C. W. (1998) in *Comprehensive Biological Catalysis* (Sinnott, M., Garner, C. D., First, E., Davies, G., Eds.) Vol. 1, Chapter 9, Academic Press, New York.
10. Hedstrom, L. (2002) Serine Protease Mechanism and Specificity, *Chem. Rev. 102*, 4501−4523.
11. Blow, D. M., Birktoft, J. J., and Hartley, B. S. (1969) Role of a Buried Acid Group in the Mechanism of Action of Chymotrypsin, *Nature 221*, 337−340.
12. Robillard, G., and Shulman, R. G. (1972) High-Resolution Nuclear Magnetic Resonance Study of the Histidine-Aspartate Hydrogen Bond in Chymotrypsin and Chymotrypsinogen, *J. Mol. Biol. 71*, 507−511.
13. Robillard, G., and Shulman, R. G. (1974) High-Resolution Nuclear Magnetic Resonance Studies of the Active Site of Chymotrypsin 2. Polarization of Histidine 57 by Substrate Analogues and Competitive Inhibitors, *J. Mol. Biol. 86*, 541−558.
14. Bachovchin, W. W., and Roberts, J. D. (1978) Nitrogen-15 Nuclear Magnetic Resonance Spectroscopy. The State of Histidine in the Catalytic Triad of α-Lytic Protease. Implications for the Charge-Relay Mechanism of Peptide-Bond Cleavage by Serine Proteases, *J. Am. Chem. Soc. 100*, 8041−8047.
15. Bachovchin, W. W. (1985) Confirmation of the assignment of the low-field proton resonance of serine proteases by using specifically nitrogen-15 labeled enzyme, *Proc. Natl. Acad. Sci. U.S.A. 82*, 7948−7951.
16. Kossiakoff, A. A., and Spencer, S. A. (1980) Neutron diffraction identifies His57 as the catalytic base in trypsin, *Nature 288*, 414−416.
17. Kossiakoff, A. A., and Spencer, S. A. (1981) Direct Determination of the Protonation States of Aspartic Acid-102 and Histidine-57 in the Tetrahedral Intermediate of the Serine Proteases: Neutron Structure of Trypsin, *Biochemistry 20*, 6462−6474.
18. Cassidy, C. S., Lin, J., and Frey, P. A. (1997) A New Concept for the Mechanism of Action of Chymotrypsin: The Role of the Low-Barrier Hydrogen Bond, *Biochemistry 36*, 4576−4584.
19. Lin, J., Cassidy, C. S., and Frey, P. A. (1998) Correlations of the Basicity of His57 with Transition State Analogue Binding, Substrate Reactivity, and the Strength of the Low-Barrier Hydrogen Bond in Chymotrypsin, *Biochemistry 37*, 11940−11948.
20. Lin, J., Westler, W. M., Clealand, W, W., Markley, J. L, and Frey, P. A. (1998) Fractionation factors and activation energies for exchange of the low barrier hydrogen bonding proton in peptidyl trifluoromethyl ketone complexes of chymotrypsin, *Proc. Natl. Acad. Sci. U.S.A. 95*, 14664−14668.
21. Neidhart, D., Wei, Y., Cassidy, C., Lin, J., Cleland, W. W., and Frey, P. A. (2001) Correlation of Low-Barrier Hydrogen Bonding and Oxyanion Binding in Transition State Analogue Complexes of Chymotrypsin, *Biochemistry 40*, 2439−2447.
22. Westler, W. M., Frey, P. A., Lin, J., Wemmer, D. E., Morimot, H., Williams, P. G., and Markley, J. L. (2002) Evidence for a Strong Hydrogen Bond in the Catalytic Dyad of Transition-State Analogue Inhibitor Complexes of Chymotrypsin from Proton-Triton NMR Isotope Shifts, *J. Am. Chem. Soc. 124*, 4196−4197.
23. Ash, E. L., Sudmeier, J. L., De Fabo, E, C., and Bachovchin, W. W. (1997) Unusual ^{1}H NMR chemical shifts support (His) $C^{\epsilon 1}$-H...O═C H-bond: Proposal for reaction-driven ring flip mechanism in serine protease catalysis, *Science 278*, 1128−1132.
24. Westler, W. M., Weinhold, F., and Markley, J. L. (2002) Quantum Chemical Calculations on Structural Models of the Catalytic Site of Chymotrypsin: Comparison of Calculated Results with Experimental Data from NMR Spectroscopy, *J. Am. Chem. Soc. 124*, 14373−14381.
25. Gordon, M. S., Freitag, M. A., Bandyopadhyay, P., Jensen, J. H., Kairys, V., and Stevens, W. J. (2001) The Effective Fragment Potential Method: A QM-Based MM Approach to Modeling Environmental Effects in Chemistry, *J. Phys. Chem. A 105*, 293−307.
26. Molina, P. A., Sikorski, R. S., and Jensen, J. H. (2003) NMR Chemical Shifts in the Low-pH form of α-chymotrypsin. A QM/MM and ONIOM-NMR Study, *Theor. Chem. Acc. 109*, 100−107.
27. Molina, P. A., and Jensen, J. H. (2003) A Predictive Model of Strong Hydrogen Bonding in Proteins: The $N^{\delta 1}$-H-$O^{\delta 1}$ Hydrogen Bond in Low-pH α-Chymotrypsin and α-Lytic Protease, *J. Phys. Chem. B 107*, 6226−6233.
28. Karadakov, P. B., and Morokuma, K. (2000) ONIOM as an efficient tool for calculating NMR chemical shielding constants in large molecules, *Chem. Phys. Lett. 317*, 589−596.
29. Monard, G., and Merz, K. M., Jr. (1999) Combined Quantum Mechanical/Molecular Mechanical Methodologies Applied to Biomolecular Systems, *Acc. Chem. Res. 32*, 904−911.

30. Field, M. J. (2002) Simulating Enzyme Reactions: Challenges and Perspectives, *J. Comput. Chem. 23*, 48−58.
31. Villà, J., and Warshel, A. (2001) Energetics and Dynamics of Enzymatic Reactions, *J. Phys. Chem. B 105*, 7887−7907.
32. Kollman, P. A., Kuhn, B., and Peräkylä, M. (2002) Computational Studies of Enzyme-Catalyzed Reactions: Where Are We in Predicting Mechanisms and in Understanding the Nature of Enzyme Catalysis?, *J. Phys. Chem. B 106*, 1537−1542.
33. Gao, J., and Truhlar, D. G. (2002) Quantum Mechanical Methods for Enzyme Kinetics, *Annu. Rev. Phys. Chem. 53*, 467−505.
34. Warshel, A., Papazyan, A., and Kollman, P. A. (1995) On Low-Barrier Hydrogen Bonds and Enzyme Catalysis, *Science 269*, 102−103.
35. Warshel, A., and Papazyan, A. (1996) Energy considerations show that low-barrier hydrogen bonds do not offer a catalytic advantage over ordinary hydrogen bonds, *Proc. Natl. Acad. Sci. U.S.A. 93*, 13665−13670.
36. Schutz, C. N., and Warshel, A. (2004) The Low Barrier Hydrogen Bond (LBHB) Proposal Revisited: The Case of the Asp ... His Pair in Serine Proteases *Proteins: Struct., Funct., Bioinf. 55*, 711−723.
37. Shokhen, M., and Albeck, A. (2004) Is There a Weak H-bond → LBHB Transition on Tetrahedral Complex Formation in Serine Proteases? *Proteins: Struct., Funct., Bioinf. 55*, 468−477.
38. Topf, M., Várnai, P., and Richards, W. G. (2002) Ab Initio QM/MM Dynamics Simulation of the Tetrahedral Intermediate of Serine Proteases: Insights into Active Site Hydrogen-Bonding Network, *J. Am. Chem. Soc. 124*, 14780−14788.
39. Ishida, T., and Kato, S. (2003) Theoretical Perspectives on the Reaction Mechanism of Serine Proteases: The Reaction Free Energy Profiles of the Acylation Process, *J. Am. Chem. Soc. 125*, 12035−12048.
40. Ishida, T., and Kato, S. (2004) Role of Asp102 in the Catalytic Relay System of Serine Proteases: A Theoretical Study, *J. Am. Chem. Soc. 126*, 7111−7118.
41. Jameson, C. J. (1996) Understanding NMR Chemical Shifts, *Annu. Rev. Phys. Chem. 47*, 135−169.
42. Helgaker, T., Jaszuñski, M., and Ruud, K. (1999) Ab initio Methods for the Calculation of NMR Shielding and Indirect Spin−Spin Coupling Constants, *Chem. Rev. 99*, 293−352.
43. Gauss, J. (2000) in *Modern Methods and Algorithms of Quantum Chemistry* (Grotendorst, J., Ed.) Proceedings, 2nd ed., John von Neumann Institute for Computing, Jülich.
44. Oldfield, E. (2002) Chemical Shifts in Amino Acids, Peptides, and Proteins: From Quantum Chemistry to Drug Design, *Annu. Rev. Phys. Chem. 53*, 349−378.
45. Mikkelsen, K. V., Jørgensen, P., Ruud, K., and Helgaker, T. (1997) A multipole reaction-field model for gauge-origin independent magnetic properties of solvated molecules, *J. Chem. Phys. 106*, 1170−1180.
46. Cammi, R., Mennucci, B., and Tomasi, J. (1999) Nuclear magnetic shielding in solution: Gauge invariant atomic orbital calculation using the polarizable continuum model, *J. Chem. Phys. 110*, 7627−7638.
47. Cui, Q., and Karplus, M. (2000) Molecular Properties from Combined QM/MM Methods. 2. Chemical Shifts in Large Molecules, *J. Phys. Chem. B 104*, 3721−3743.
48. Yamazaki, T., Sato, H., and Hirata, F. (2001) Solvent effect on the nuclear magnetic shielding: ab initio study by the combined reference interaction site model and electronic structure theories, *J. Chem. Phys. 115*, 8949−8957.
49. Ditchfield, R. (1974) Self-consistent perturbation theory of diamagnetism 1. A gauge-invariant LCAO method for N.M.R. chemical shifts, *Mol. Phys. 27*, 789−807.
50. Wolinski, K., Hinton, J. F., and Pulay, P. (1990) Efficient Implementation of the Gauge-Independent Atomic Orbital Method for NMR Chemical Shift Calculations, *J. Am. Chem. Soc. 112*, 8251−8260.
51. Cornell, W. D., Cieplak, P., Bayly, C. I., Gould, I. R., Merz, K. M., Jr., Ferguson, D. M., Spellmeyer, D. C., Fox, T., Caldwell, J. W., and Kollman, P. A. (1995) A Second Generation Force Field for the Simulation of Proteins, Nucleic Acids, and Organic Molecules, *J. Am. Chem. Soc. 117*, 5179−5197.
52. Kollman, P., Dixon, R., Cornell, W., Fox, T., Chipot, C., and Pohorille, A. (1997) in *Computer Simulation of Biomolecular Systems* (van Gunsteren, W. F., Weiner, P. K., Wilkinson, A. J., Eds.) Vol. 3, Kluwer Academic Publishers, New York.
53. Yamaguchi, Y., Osamura, Y., Goddard, J. D., and Schaefer, H. F., III (1994) *A New Dimension to Quantum Chemistry: analytic derivative methods in ab initio molecular electronic structure theory*, Oxford, New York.
54. Zhang, Y., Liu, H., and Yang, W. (2000) Free energy calculation on enzyme reactions with an efficient iterative procedure to determine minimum energy paths on a combined ab initio QM/MM potential energy surface, *J. Chem. Phys. 112*, 3483−3492.
55. Liu, H., Zhang, Y., and Yang, W. (2000) How Is the Active Site of Enolase Organized To Catalyze Two Different Reaction Steps?, *J. Am. Chem. Soc. 122*, 6560−6570.
56. Cisneros, G. A., Liu, H., Zhang, Y., and Yang, W. (2003) Ab initio QM/MM Study Shows There Is No General Acid in the Reaction Catalyzed by 4-Oxalocrotonate Tautomerase, *J. Am. Chem. Soc. 125*, 10384−10393.
57. Bayly, C. I., Cieplak, P., Cornell, W. D., and Kollman, P. A. (1993) A Well-Behaved Electrostatic Potential Based Method Using Charge Restraints for Deriving Atomic Charges: The RESP Model, *J. Phys. Chem. 97*, 10269−10280.
58. Cieplak, P., Cornell, W. D., Bayly, C., and Kollman, P. A. (1995) Application of the Multimolecule and Multiconformational RESP Methodology to Biopolymers: Charge Derivation for DNA, RNA, and Proteins, *J. Comput. Chem. 16*, 1357−1377.
59. Kollman, P. (1993) Free Energy Calculations: Applications to Chemical and Biochemical Phenomena, *Chem. Rev. 93*, 2395−2417.
60. Hehre, W. J., Radom, L., van Schleyer, P. R., and Pople, J. A. (1986) *Ab Initio Molecular Orbital Theory*, John Wiley & Sons, Inc., New York.
61. Kendall, R. A., Dunning, T. H., and Harrison, R. J. (1992) Electron affinities of the first-row atoms revisited. Systematic basis sets and wave functions, *J. Chem. Phys. 96*, 6796−6806.
62. Bachovchin, W. W. (1986) ^{15}N NMR Spectroscopy of Hydrogen-Bonding Interactions in the Active Site of Serine Proteases: Evidence for a Moving Histidine Mechanism, *Biochemistry 25*, 7751−7759.
63. Bachovchin, W. W., Wong, W. Y. L., Farr-Jones, S., Shenvi, A. B., and Kettner, C. A. (1988) Nitrogen-15 NMR Spectroscopy of the Catalytic-Triad Histidine of a Serine Protease in Peptide Boronic Acid Inhibitor Complexes, *Biochemistry 27*, 7689−7697.
64. Sudmeier, J. L., Bradshaw, E. M., Coffman Haddad, K. E., Day, R. M., Thalhauser, C. J., Bullock, P. A., and Bachovchin, W. W. (2003) Identification of Histidine Tautomers in Proteins by 2D ^{1}H/^{13}C$^{\delta 2}$ One-Bond Correlated NMR, *J. Am. Chem. Soc. 125*, 8430−8431.
65. Barich, D. H., Nicholas, J. B., and Haw, J. F. (2001) Gauge-Including Atomic Orbital Proton Chemical Shifts of Strong Hydrogen Bonds: The Importance of Electron Correlation, *J. Phys. Chem. A 105*, 4708−4715.
66. Garcia-Viloca, M., Gelabert, M., González-Lafont, A., Moreno, M., and Lluch, J. M. (1997) Is an Extremely Low-Field Proton Signal in the NMR Spectrum Conclusive Evidence for a Low-Barrier Hydrogen Bond?, *J. Phys. Chem. A 101*, 8727−8733.
67. Derewenda, Z. S., Derewenda, U., and Kobos, P. M. (1994) (His) C$^{\epsilon}$-H ... O═C Hydrogen Bond in the Active Sites of Serine Hydrolases, *J. Mol. Biol. 241*, 83−93.
68. Haddad, K. C., Sudmeier, J. L., Bachovchin, D. A., and Bachovchin, W. W. (2005) α-Lytic protease can exit in two separately stable conformations with different His57 mobilities and catalytic activities, *Proc. Natl. Acad. Sci. U.S.A. 102*, 1006−1011.

BI051515B